Supporting Information

Imada et al. 10.1073/pnas.1001866107

SI Materials and Methods

Bacterial Strains, Plasmids, DNA Manipulations, and Media. The bacterial strains and plasmids used in this study are listed in Table S1. DNA manipulations, site-directed mutagenesis, and DNA sequencing were carried out as described previously (1). LB and soft tryptone agar plates were used as described previously (2).

Purification of Proteins. Details of expression and purification of FliT and FliD have been described previously (3, 4). The FliT–FliD complex was prepared by mixing purified FliT (1–1.5 mg/mL) and FliD (8–10 mg/mL) with a molar ratio of 1:1. The mixture was loaded onto a Hi-Load Superdex 75 (26/60) column (GE Healthcare) equilibrated with 10 mM Hepes-NaOH (pH 7.0). Fractions corresponding to the FliT–FliD complex were pooled and concentrated for further use.

Crystal Structure Determination. Details of crystallization of FliT have been described previously (3). In brief, trigonal $P3_121$ crystals of SeMet FliT with unit cell dimensions a = b =121.3 Å and c = 58.7 Å were grown from a solution containing 1.0 M potassium/sodium tartrate, 200 mM $LiSO_4$, and 0.1 M CHES-NaOH (pH 9.5) by the sitting drop vapor diffusion method. X-ray diffraction data were collected at the synchrotron beamline BL41XU of SPring-8 with the approval of the Japan Synchrotron Radiation Research Institute (Proposals 2006B1058 and 2008A1402). The statistics of the data have been reported previously (3). The diffraction data were collected under a helium gas flow at 35 K to reduce the radiation damage. The data were processed with MOSFLM (5) and scaled with SCALA (6). Phase calculation was performed using SOLVE (7). The electron density map was calculated from SAD phases from the Se-Met derivative data, followed by density modification with DM (6). The model was built with Coot (8) and refined at 3.2 Å using the CNS program (9). During the refinement process, iterative manual modifications were carried out using "omit map." The refinement converged to an *R* factor of 25.2% and a free *R* factor of 28.6%. The Ramachandran plot indicated that 92.8% and 7.2% residues were located in the most favorable and allowed regions, respectively. Structural refinement statistics are summarized in Table S2.

Size-Exclusion Column Assay. Size-exclusion column assay for FliT was carried out with a Superdex 200 HR 10/30 column (GE Healthcare) in three different solution conditions: (i) 50 mM Hepes-NaOH (pH 7) with 150 mM NaCl, (ii) 50 mM Hepes-NaOH (pH 7) with 500 mM NaCl, and (iii) 50 mM CAPS-NaOH (pH 10) with 150 mM NaCl. A 100-μL solution of FliT (2.4 mg/mL) equilibrated to each condition was loaded onto the column and eluted with a flow rate of 0.5 mL/min. The size marker size marker proteins were albumin (67 kDa), ovalbumin (44 kDa), chymotrypsinogen A (25 kDa), and ribonuclease A (13.7 kDa).

Size-exclusion column assay for the FliD–FliT complex was performed with a Superose 12 HR 10/30 column (GE Healthcare) equilibrated with 10 mM Tris-HCl (pH 7.8).

The sample solutions were prepared by mixing purified FliT and FliD at molar ratios of 1:0, 2:1, 1:1, 0.5:1, and 0:1. The final concentration of FliD was adjusted to 15 μM for the 2:1, 1:1, 0.5:1, and 0:1 mixtures. A 500-μL solution of each mixture was applied onto the column and eluted with a flow rate of 0.5 mL/min.

Sedimentation Equilibrium Analysis. Sedimentation equilibrium measurement was conducted using a Beckman Coulter Optima XL-A Ultracentrifuge with an AnTi 60 rotor. The purified samples of FliT and the FliT–FliD complex were dialyzed against a solution containing 50 mM Hepes-NaOH (pH 7.0) and 150 mM NaCl and a solution containing 10 mM Hepes-NaOH (pH 7.0) and 150 mM NaCl, respectively. The sample solutions were filled in a two-channel charcoal-filled epon cell with quartz windows. The sedimentation data for FliT were collected at 20 °C at speeds of 30,000, 32,000, and 34,000 rpm at initial concentrations of 0.18 mg/mL, 0.27 mg/mL, and 0.45 mg/mL, respectively. The data for the FliT–FliD complex were collected at 20 °C at speeds of 10,000, 12,000, 14,000, and 16,000 rpm. The initial concentration was adjusted at an OD_{280} of 0.2. The sedimentation profiles were acquired by scanning the optical absorbance at a wavelength of 280 nm with a spacing of 0.001 cm in step mode, with 20 averages per step. The data were analyzed using Beckman Coulter Optima XL-A/XL-I data analysis software, version 4.0. The partial specific volumes (0.739 mL/g for FliT and 0.733 mL/g for the complex) were calculated based on the amino acid compositions of the proteins and used for the analysis.

Swarming Motility Assay. Fresh colonies were inoculated onto soft tryptone agar plates and incubated at 30 °C as described previously (10).

Pull-Down Assays by GST Affinity Chromatography. WT cells expressing GST, GST-FliT, or GST-FliT94 were suspended in PBS [8 g of NaCl, 0.2 g of KCl, 3.63 g of $Na_2HPO_4 \bullet 12H_2O$, and 0.24 g of KH_2PO_4 (pH 7.4)/L] and sonicated. After the cell lysates were centrifuged to remove undisrupted cells and insoluble membrane fractions, the soluble fractions were loaded onto a GST agarose column (GE Healthcare). After the column was washed thoroughly with PBS, proteins were eluted with 50 mM Tris-HCl (pH 8.0) and 10 mM reduced glutathione. Fractions containing GST, GST-FliT, or GST-FliT94 were indentified by SDS/PAGE with CBB staining.

For copurification of His-FliH, His-FliI, His-FliJ, or FliD with GST-FliT or GST-FliT94, the soluble fractions prepared from a Δ*flhDC-cheW* mutant expressing GST-FliT or GST-FliT94 were mixed with those from the Δ*flhDC-cheW* mutant transformed with pMM306 (His-FliH), pMM1702 (His-FliI), pMM406 (His-FliJ), or pMMD001 (FliD). The mixtures were loaded onto the GST affinity column. After washing, bound proteins were eluted.

For copurification of His-FliI and His-FliJ with the GST-FliT94–GST-FliD complex, purified His-FliI and His-FliJ were incubated overnight with purified GST-FliT94–GST-FliD complex at 4 °C, after which the mixtures were loaded onto the GST affinity column. After washing, bound proteins were eluted.

After SDS/PAGE, immunoblotting with polyclonal anti-FlhD, anti-FlhC, anti-FliH, anti-FliI, anti-FliJ, and anti-FliD antibodies was carried out as described previously (2). Proteins were detected with an ECL immunoblotting detection kit (GE Healthcare).

1. Saijo-Hamano Y, Minamino T, Macnab RM, Namba K (2004) Structural and functional analysis of the C-terminal cytoplasmic domain of FlhA, an integral membrane component of the type III flagellar protein export apparatus in *Salmonella*. *J Mol Biol* 343:457–466.
2. Minamino T, Macnab RM (1999) Components of the *Salmonella* flagellar export apparatus and classification of export substrates. *J Bacteriol* 181:1388–1394.
3. Kinoshita M, et al. (2009) Purification, crystallization and preliminary X-ray analysis of FliT, a bacterial flagellar substrate-specific export chaperone. *Acta Crystallogr F* 65: 825–828.
4. Imada K, Vonderviszt F, Furukawa Y, Oosawa K, Namba K (1998) Assembly characteristics of flagellar cap protein HAP2 of *Salmonella*: Decamer and pentamer in the pH-sensitive equilibrium. *J Mol Biol* 277:883–891.

5. Leslie AGW (1992) CCP4 + ESF – EACMB. *Newslett Protein Crystallogr* 26:27–33.
6. Collaborative Computational Project, Number 4 (1994) The CCP4 suite: Programs for protein crystallography. *Acta Crystallogr D* 50:760–763.
7. Terwilliger TC, Berendzen J (1999) Automated MAD and MIR structure solution. *Acta Crystallogr D* 55:849–861.
8. Emsley P, Cowtan K (2004) Coot: Model-building tools for molecular graphics. *Acta Crystallogr D* 60:2126–2132.
9. Brünger AT, et al. (1998) Crystallography & NMR system: A new software suite for macromolecular structure determination. *Acta Crystallogr D* 54:905–921.
10. Minamino T, MacNab RM (2000) Interactions among components of the *Salmonella* flagellar export apparatus and its substrates. *Mol Microbiol* 35:1052–1064.
11. Yamaguchi S, Fujita H, Sugata K, Taira T, Iino T (1984) Genetic analysis of H2, the structural gene for phase-2 flagellin in *Salmonella*. *J Gen Microbiol* 130:255–265.
12. Ohnishi K, Ohto Y, Aizawa S, Macnab RM, Iino T (1994) FlgD is a scaffolding protein needed for flagellar hook assembly in *Salmonella typhimurium*. *J Bacteriol* 176: 2272–2281.
13. Stebbins CE, Galán JE (2001) Maintenance of an unfolded polypeptide by a cognate chaperone in bacterial type III secretion. *Nature* 414:77–81.
14. Büttner CR, Sorg I, Cornelis GR, Heinz DW, Niemann HH (2008) Structure of the *Yersinia enterocolitica* type III secretion translocator chaperone SycD. *J Mol Biol* 375:997–1012.
15. Quinaud M, et al. (2007) Structure of the heterotrimeric complex that regulates type III secretion needle formation. *Proc Natl Acad Sci USA* 104:7803–7808.

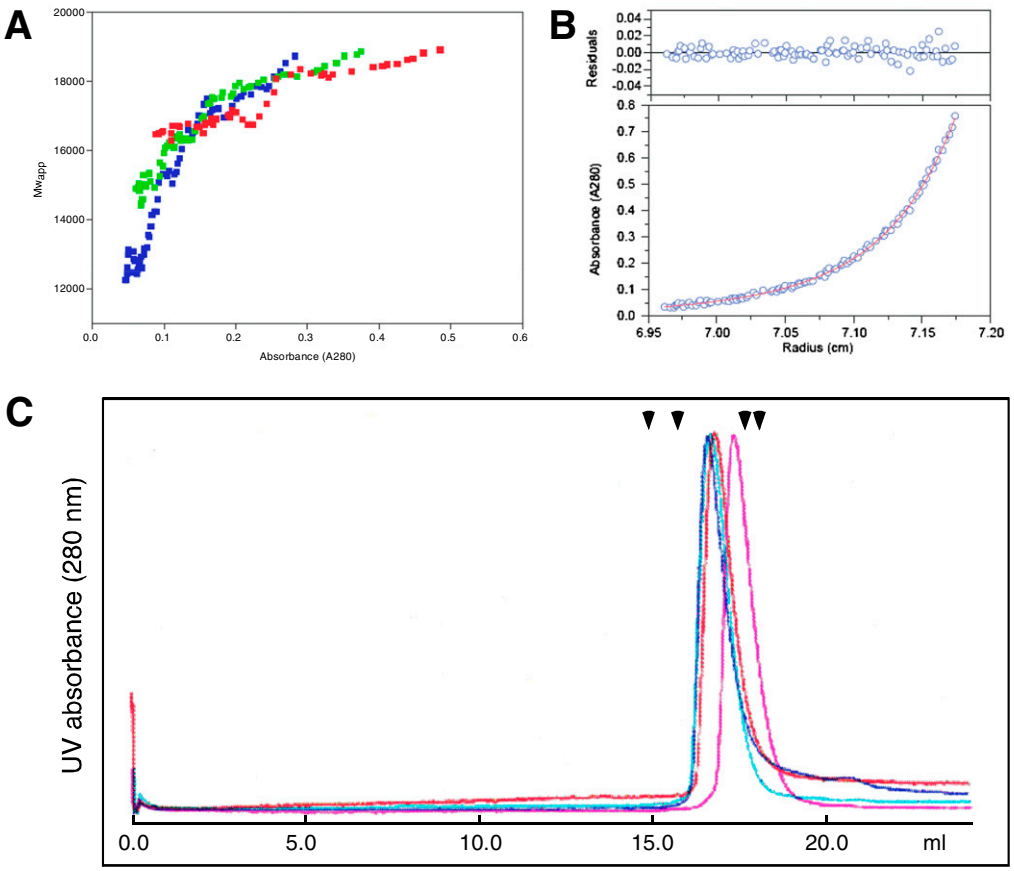

Fig. S1. Characterization of FliT in solution. (*A* and *B*) Sedimentation equilibrium measurement of FliT. (*A*) Protein concentration dependence of the apparent molecular weight (Mw_{app}) calculated from the data measured at 32,000 rpm at initial protein concentration of 0.18 mg/mL (blue dots), 0.27 mg/mL (green dots), and 0.45 mg/mL (red dots). (*B*) (*Lower*) An example of the sedimentation equilibrium profile (initial absorbance at 280 nm of 0.3, measured at 32,000 rpm). The open circles are data points, and the continuous red line is a model fit curve for a monomer-dimer system. The best-fitting curve was derived from the global fitting method using the data of six different conditions. (*Upper*) Plots of the residuals of each data point from the fitting curve. (*C*) Elution profiles of FliT in various solutions. The blue line denotes 50 mM HEPES-NaOH (pH 7) with 150 mM NaCl; the cyan line, 50 mM CAPS-NaOH (pH 10) with 150 mM NaCl; the red line, 50 mM HEPES-NaOH (pH 7) with 500 mM NaCl; the pink line, 50 mM CHES-NaOH (pH 7) with 200 mM K/Na tartrate and 100 mM Li_2SO4 (crystallization condition). Arrows indicate the elution peaks of the size marker proteins: albumin (67 kDa), ovalbumin (44 kDa), chymotrypsinogen A (25 kDa) and ribonuclease A (13.7 kDa) at 14.9 mL, 15.7 mL, 17.7 mL, and 18.1 mL, respectively.

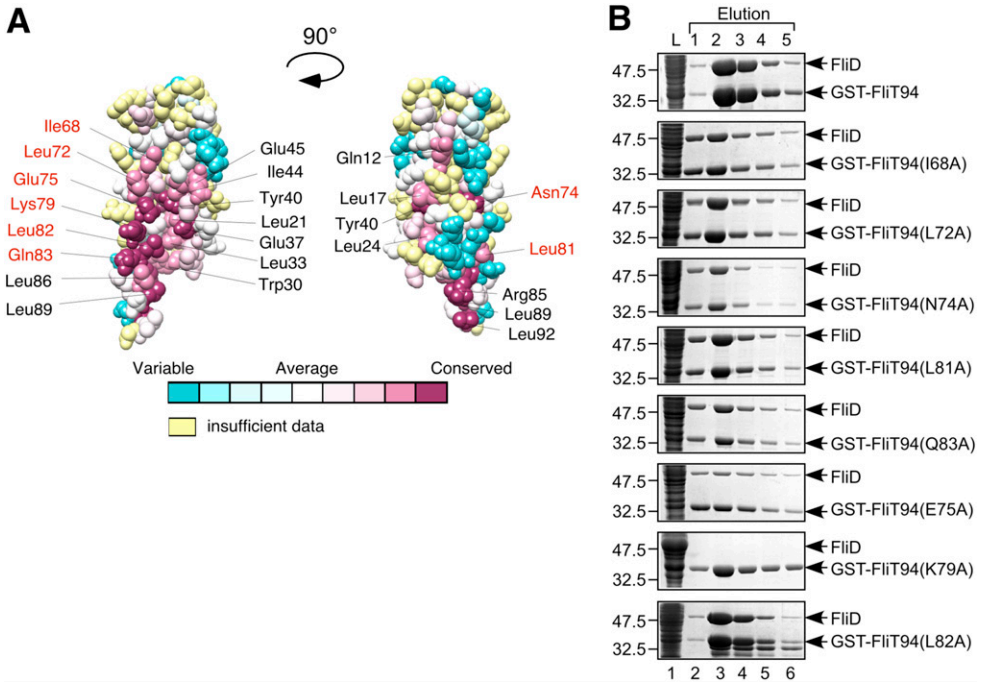

Fig. S2. Interaction of FliD with various Ala-substituted forms of GST-FliT94. (*A*) Evolutionary conserved residues of FliT94. Residues substituted to alanine were labeled with red and other highly conserved surface-exposed residues are labeled with black. The figure was prepared by ConSurf (http://consurf.tau.ac.il/). Residues are colored in accordance with conservation among amino acid sequences of FliT from 55 different bacteria. (*B*) Soluble fractions (designated L) prepared from a Δ*flhDC-cheW* mutant expressing GST-FliT94 (first row), GST-FliT94(I68A) (second row), GST-FliT94(L72A) (third row), GST-FliT94(N74A) (fourth row), GST-FliT94(L81A) (fifth row), GST-FliT(Q83A) (sixth row), GST-FliT(E75A) (seventh row), GST-FliT94(K79A) (eighth row), or GST-FliT94(L82A) (ninth row) were loaded onto a GST column. After extensive washing with PBS, FliD was loaded onto the column and well mixed for 1 h. After washing with 20 mL PBS, proteins were eluted with a buffer containing 10 mM reduced glutathione. The eluted fractions were analyzed by CBB staining.

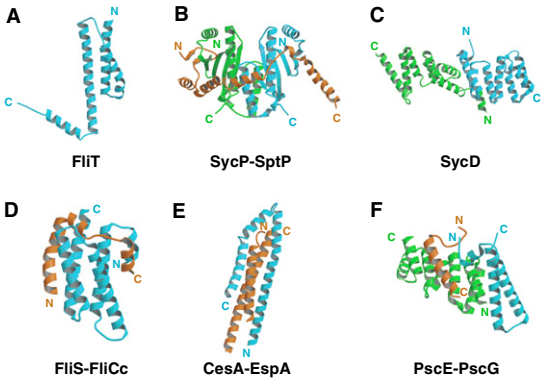

Fig. S3. Comparison of the type III–specific chaperone structures. Cα ribbon diagrams of FliT and the representative chaperons in five different classes are shown: (*A*) MolA of FliT, (*B*) SycP (class I) in complex with SptP (PDB ID: 1JYO), (*C*) SycD (class II) (PDB ID: 2VGX), (*D*) FliS (class III) in complex with the C-terminal fragment of FliC (PDB ID: 1ORY), (*E*) CesA (class IV) in complex with EspA (PDB ID: 1XOU), and (*F*) PscE (class V)–PscG in complex with PscF (PDB ID: 2UWJ). The chaperon molecules are in cyan and green, and the secretion substrates are in orange. SycP (*B*) and SycD (*C*) form homodimers (13, 14). PscE (*F*) forms a heterodimer with its cochaperone PscG (15), shown in cyan and green, respectively.

Table S1. Strains and plasmids used in this study

Strains and plasmids	Relevant characteristics	Source or reference
Salmonella		
SJW1103	WT for motility and chemotaxis	(11)
SJW1368	Δ(*cheW-flhD*); master operon mutant	(12)
Plasmids		
pGEX-6p-1	Expression vector	GE Healthcare
pMM306	pTrc99A/His-FliH	(10)
pMM406	pTrc99A/His-FliJ	(10)
pMM1702	pTrc99A/His-FliI	(10)
pMMD001	pTrc99A/FliD	This study
pMMT001	pGEX-6p-1/GST-FliT	This study
pMMT002	pGEX-6p-1/GST-FliT94	This study
pMMT002(I68A)	pGEX-6p-1/GST-FliT94(I68A)	This study
pMMT002(L72A)	pGEX-6p-1/GST-FliT94(L72A)	This study
pMMT002(N74A)	pGEX-6p-1/GST-FliT94(N74A)	This study
pMMT002(E75A)	pGEX-6p-1/GST-FliT94(E75A)	This study
pMMT002(K79A)	pGEX-6p-1/GST-FliT94(K79A)	This study
pMMT002(L81A)	pGEX-6p-1/GST-FliT94(L81A)	This study
pMMT002(L82A)	pGEX-6p-1/GST-FliT94(L82A)	This study
pMMT002(Q83A)	pGEX-6p-1/GST-FliT94(Q83A)	This study

Table S2. X-ray refinement statistics

Resolution range, Å	42.2–3.2	(3.4–3.2)
Number of reflections working	7,550	(1,237)
Number of reflections test	826	(132)
R_w, %	25.2	(31.7)
R_{free}, %	28.6	(35.9)
rms deviation bond length, Å	0.010	
rms deviation bond angle, degrees	1.5	
B-factors		
Protein atoms	52.4	
Ramachandran plot (%)		
Most favored	92.8	
Additionally allowed	7.2	
Generously allowed	0	
Disallowed	0	
Number of protein atoms	1,849	
Number of solvent atoms	0	

Values in parentheses are for the highest-resolution shell. $R_w = \Sigma \| Fo | - | Fc \| / \Sigma | Fo |$; $R_{free} = \Sigma \| Fo | - | Fc \| / \Sigma | Fo |$.